Nonlinear dynamos at infinite magnetic Prandtl number

Alexandros Alexakis
Laboratoire de Physique Statistique de l'Ecole Normale Supérieure, UMR CNRS 8550, 24 Rue Lhomond, F-75006 Paris Cedex 05, France
(Received 29 October 2010; published 3 March 2011)

The dynamo instability is investigated in the limit of infinite magnetic Prandtl number. In this limit the fluid is assumed to be very viscous so that the inertial terms can be neglected and the flow is enslaved to the forcing. The forcing consist of an external forcing function that drives the dynamo flow and the resulting Lorentz force caused by the back reaction of the magnetic field. The flows under investigation are the Archontis flow and the ABC flow forced at two different scales. The investigation covers roughly 3 orders of magnitude of the magnetic Reynolds number above onset. All flows show a weak increase of the averaged magnetic energy as the magnetic Reynolds number is increased. Most of the magnetic energy is concentrated in flat elongated structures that produce a Lorentz force with small solenoidal projection so that the resulting magnetic field configuration is almost force free. Although the examined system has zero kinetic Reynolds number at sufficiently large magnetic Reynolds number the structures are unstable to small scale fluctuations that result in a chaotic temporal behavior.

DOI: 10.1103/PhysRevE.83.036301 PACS number(s): 47.65.−d, 05.45.−a, 91.25.Cw

Dynamo instability is considered to be the main mechanism for the generation and sustainment of magnetic field throughout the universe [1]. In this scenario an initially small magnetic field is amplified by currents induced solely by the motion of a conducting fluid. This process saturates when the magnetic field becomes strong enough for the Lorentz force to act back on the flow and reduce its ability to further amplify the magnetic energy. The exact effect the Lorentz force has on the flow and which property of the flow is altered to prevent further magnetic field amplification is the subject of many current investigations.

One can in principle envision many scenarios for saturation especially in the presence of turbulence. For example, saturation can occur because the magnetic field suppresses the fluid flow thus reducing the magnetic Reynolds number of the flow to its critical value. This behavior is expected close to the dynamo onset for laminar flows. In another scenario, dynamo can saturate by suppressing the chaotic stretching of the magnetic field lines [2,3], or the dynamo can saturate because the folding of the field lines is modified to be less constructive. Finally, saturation of the dynamo can be due to correlations between the velocity and the magnetic field without suppressing the ability of the flow to amplify an uncorrelated passive vector field and thus in principle still be a dynamo flow (see for example [4–6] and discussion in [7]).

In principle there is no unique answer to this question and the list above does not exhaust all possibilities. The exact mechanism can be a combination of different processes whose choice can depend on the type of forcing and the examined parameter range. Identifying the mechanisms in simple flows can help in unveiling the dependence of the amplitude of magnetic field saturation on the magnetic Reynolds number R_m and the fluid Reynolds number Re. This dependence is important for astrophysics, bearing in mind that both numbers are very large, with $1 \ll R_m \ll \mathrm{Re}$ for the Sun and $1 \ll \mathrm{Re} \ll R_m$ for the galaxy.

In this large parameter space, it is interesting to examine special limits of the governing equations, in order to obtain a basic understanding of nonlinear dynamo behavior. This is attempted in this work. Here saturated dynamos are investigated in the simplified limit of large viscosity. In this system the inertial terms can be neglected and the resulting flow is a Stokes flow driven by the external force and the Lorentz force. This limit is typically used as a model for the small scale galactic dynamo for which the magnetic Prandtl number (which is equal to the ratio of the viscosity to the magnetic diffusivity) is very large. In previous investigations [8–11] the forcing was assumed random and changing in time in order to model turbulent fluctuations at the viscous cutoff scale. The turbulent fluctuations at this scale result in the fastest growing dynamo modes at the kinematic stage of the dynamo. Here the opposite limit is examined and a time independent forcing is used. A steady forcing might not be suitable in describing the turbulent velocity fluctuations; however it allows us to investigate the reaction of the magnetic field to large scale flows with long time correlations that could be more relevant in the saturated stage. Another interesting property of this limit is that the system is stripped of all hydrodynamic instabilities. Thus, when comparing with the results of turbulent magnetohydrodynamic (MHD) flows one can distinguish which effect is due to turbulence and hydrodynamic instabilities and which solely due to the effect of the Lorentz force.

This paper is structured as follows: The next section describes the dynamical equations in the limit considered. Section II explains the numerical method and its limitations. Section III describes the results for each of the examined flows. Section IV gives some common scaling laws observed for all flows, and conclusions are drawn in the last section.

I. EQUATIONS AND SETUP

We consider flows in a triple periodic domain of size $L = 2\pi$ driven by a simple time independent body force. The nondimensional MHD equations for a unit density fluid are then given by

$$\mathrm{Re}(\partial_t \mathbf{u} + \mathbf{u}\cdot\nabla\mathbf{u}) = \mathbf{b}\cdot\nabla\mathbf{b} - \nabla P + \nabla^2\mathbf{u} + \mathbf{F}, \qquad (1)$$

$$\partial_t \mathbf{b} + \mathbf{u}\cdot\nabla\mathbf{b} = \mathbf{b}\cdot\nabla\mathbf{u} + \frac{1}{R_m}\nabla^2\mathbf{b}. \qquad (2)$$

F is the external body force that in the absence of magnetic fields sustains a velocity field **u**, of unity root mean squared value $U = \langle \mathbf{u^2} \rangle^{1/2}|_{\mathbf{b=0}} = 1.0$ (where $\langle\cdot\rangle$ stands for spatial average). The Reynolds number is defined as $\mathrm{Re} = UL/(2\pi\nu)$ where ν is the kinematic viscosity and we are going to consider the limit $\mathrm{Re} \ll 1$. The magnetic field is expressed by $\mathbf{b} = \sqrt{\mathrm{Re}}\tilde{\mathbf{b}}/U$, where $\tilde{\mathbf{b}}$ is the dimensional magnetic field measured in units of velocity. The factor of $\sqrt{\mathrm{Re}}$ has been introduced to set the Lorentz force (which leads to saturation) to the same order of magnitude as the forcing term. The magnetic Reynolds number is defined as $R_m = UL/(2\pi\eta)$, where η is the magnetic diffusivity. P is the pressure that ensures the incompressibility condition $\nabla \cdot \mathbf{u} = 0$.

We are interested in the limit $\mathrm{Re} \ll 1$ while R_m is still finite; thus the magnetic Prandtl number P_m, defined as the ratio of the two Reynolds numbers $P_m \equiv R_m/\mathrm{Re} = \nu/\eta$, tends to infinity. In this limit then, the left hand side of Eq. (1) can be dropped and the velocity field is enslaved to the forcing and the Lorentz force and is given by

$$\mathbf{u} = -\nabla^{-2}[\mathbf{b} \cdot \nabla\mathbf{b} - \nabla P + \mathbf{F}], \tag{3}$$

where ∇^{-2} stands for the inverse Laplacian. Equation (3) represents the Stokes flow of a viscous fluid under the influence of the body force **F** and the solenoidal projection of the Lorentz force $F_{j\times b} = \mathbf{b} \cdot \nabla\mathbf{b} - \nabla P$. The approximations made here are valid in the small Reynolds number limit provided that the velocity gradients do not become too sharp or the velocity time scale too short. In the examined calculations the velocity field appears to have a smooth behavior both in time and space as R_m is increased, so this condition is not violated. Equations (2) and (3) form a closed set of equations that are under investigation in this work. They are going to be referred to as the infinite magnetic Prandtl number equations. For a fixed functional form of the forcing, R_m is the only control parameter in the system. Due to the linear relation between the velocity and the forcing, R_m can also be interpreted as the magnetic Grashof number, a nondimensional measure of the forcing amplitude.

The evolution equation for the magnetic energy is given by

$$\frac{1}{2}\partial_t\langle b^2\rangle = \langle \mathbf{b} \cdot (\nabla\mathbf{u}) \cdot \mathbf{b}\rangle - \frac{1}{R_m}\langle(\nabla b)^2\rangle. \tag{4}$$

Multiplying Eq. (3) by $\nabla^2\mathbf{u}$ space averaging and subtracting from Eq. (4) we obtain

$$\frac{1}{2}\partial_t\langle b^2\rangle = \langle \mathbf{u} \cdot \mathbf{F}\rangle - \langle(\nabla u)^2\rangle - \frac{1}{R_m}\langle(\nabla b)^2\rangle. \tag{5}$$

Equation (5) is the energy balance equation that expresses that the rate of change of magnetic energy is equal to the rate at which energy is injected into the system by $\langle \mathbf{u} \cdot \mathbf{F}\rangle$ minus the energy lost by the viscous damping $\epsilon_u \equiv \langle(\nabla u)^2\rangle$ and Ohmic dissipation $\epsilon_b \equiv \langle(\nabla b)^2\rangle/R_m$. It is worth pointing out that even in the limit $R_m \to \infty$ energy is dissipated at all scales due to the viscous term. It is also noted here that the kinetic energy of the flow does not enter the energy balance equation since **u** is an enslaved vector field. If we did add it, it would be of order Re smaller than the magnetic energy. In the remaining text we will refer to the kinetic and magnetic energy as $E_u \equiv \frac{1}{2}\langle \mathbf{u^2}\rangle$ and $E_b \equiv \frac{1}{2}\langle \mathbf{b^2}\rangle$ respectively, although for a true "dimensional" comparison between the two a factor of Re should be included (i.e., $E_{\mathrm{tot}} = E_u + E_b/\mathrm{Re}$).

The infinite magnetic Prandtl equations conserve one ideal invariant (for $R_m = \infty$): the magnetic helicity [12]. Multiplying Eq. (2) by the vector potential **a** (such that $\mathbf{b} = \nabla \times \mathbf{a}$) and space averaging we obtain

$$\frac{1}{2}\partial_t\langle \mathbf{a} \cdot \mathbf{b}\rangle = -\frac{1}{R_m}\langle \mathbf{b} \cdot \nabla \times \mathbf{b}\rangle; \tag{6}$$

the magnetic helicity $H_m \equiv \frac{1}{2}\langle \mathbf{a} \cdot \mathbf{b}\rangle$ is thus conserved for infinite R_m. For large but finite R_m this invariance is expected to be violated at scales $\ell \sim 1/\sqrt{R_m}$. Since there is no large scale source term for magnetic helicity, it can be generated or destroyed only at these small scales. In dynamo investigations the initial magnetic field is very small and thus also the initial magnetic helicity is negligible. However, a flow with positive (negative) hydrodynamic helicity will generate negative (positive) magnetic helicity in the larger scales where it will "pile up" and positive (negative) helicity in the small scales where it will be dissipated. Thus although the flow itself does not generate helicity it drives preferentially one sign of helicity to the small scales where it is dissipated. So if the saturated state is magnetically helical with one sign of helicity it implies that the opposite sign of helicity has been dissipated at the small scales.

II. NUMERICAL METHOD

The infinite magnetic Prandtl number Eqs. (2) and (3) were solved in a triple periodic domain of size $L = 2\pi$ using a standard pseudospectral method and a third order in time Runge-Kutta. The code was based on a full MHD code [13,14]. The truncated fields were de-aliased every time a quadratic nonlinear term was calculated based on the 2/3 rule.

The resolution used varied from 64^3 up to 256^3 grid points. With a resolution of 256^3 one can typically achieve magnetic Reynolds numbers of the order of a few hundreds for the kinematic problem depending on the flow. However, in the nonlinear regime, the velocity amplitude is significantly reduced (in some cases by 2 orders of magnitude) and the magnetic energy is dissipated also by the viscous term making the flow less efficient at generating small scales. Thus, although at the examined resolution only magnetic Reynolds numbers of a few hundred can be reached for the kinematic problem, for the nonlinear problem magnetic Reynolds numbers of a few thousand can easily be achieved if the initial conditions were also at the nonlinear stage. The following procedure was used for the numerical runs that were performed: Starting from a well resolved kinematic dynamo simulation (very small initial magnetic field) the system was evolved until nonlinear saturation was reached. The output of this run was then used as initial conditions for the next run at a higher magnetic Reynolds number. In many cases a random perturbation was also added in the initial conditions. A run was considered well resolved if the maximum of the current density spectrum was sufficiently larger than the value of the current density spectrum at the smallest resolved scale (typically by an order of magnitude).

The strongest limitation in these runs turned out to be the time of integration. Although large magnetic Reynolds numbers can be be examined in this limit, with growth rates

of the order of the inverse turnover time, the magnetic field with large Prandtl number has much longer memory time than a typical turbulent flow. Thus to achieve saturation each run has to be integrated for time scales of the order of the diffusion time.

III. THE EXAMINED FLOWS

Three different forcing functions F were used to generate the dynamo flows. The first two are members of the ABC family:

$$\begin{aligned} u_x &= A\sin(k_f z) + B\cos(k_f y), \\ u_y &= C\sin(k_f x) + A\cos(k_f z), \\ u_z &= B\sin(k_f y) + C\cos(k_f x). \end{aligned} \tag{7}$$

The ABC flows have been extensively investigated in the literature [15–17], especially for their relevance in dynamo theory [18–21]. They are fully helical satisfying ($\nabla \times \mathbf{u} = -k_f \mathbf{u}$). Here the case for $A = B = C = 1/\sqrt{3}$ is investigated for $k_f = 1$ and for the case $k_f = 2$.

The third flow under investigation is a variation of the ABC family where only the cosine terms are kept:

$$\begin{aligned} u_x &= A\cos(k_f y), \\ u_y &= B\cos(k_f z), \\ u_z &= C\cos(k_f x). \end{aligned} \tag{8}$$

This flow was first investigated in [22,23] and was shown to result in dynamo with large saturation amplitudes of the magnetic field [24–28]. This flow will be referred as the Archontis flow. Unlike the ABC flows, it has zero global helicity. The performed runs in this work have $A = B = C = \sqrt{2/3}$ and $k_f = 1$.

IV. RESULTS

A. Archontis flow

We begin with the nonhelical Archontis flow. Figure 1 shows the saturation values of the magnetic energy $E_b = \frac{1}{2}\|\mathbf{b}\|^2$ (squares) and of the kinetic energy $E_u = \frac{1}{2}\|\mathbf{u}\|^2$ (diamonds) as a function of the magnetic Reynolds number R_m. For small values of R_m there is no dynamo and thus $\|\mathbf{b}\|^2 = 0$ and $\|\mathbf{u}\|^2 = 1$. The onset of the dynamo instability is at $R_{mc} \simeq 42.5$. For small deviations from this critical value the magnetic energy grows as $E_b \sim (R_m - R_{mc})$ as a normal mode expansion would predict [29,30], and the kinetic energy sharply decreases. The dynamo is stationary at this stage. As R_m is further increased the system goes through a series of bifurcations that we do not fully explore here. There is another critical value $R'_{mc} \simeq 80$ after which the evolution of the magnetic energy appears to be chaotic. We avoid using the term turbulence since the flow is in the small Re regime; however many common features with turbulence like power-law scalings are present in this regime. It is noted that this chaotic state does not result from a random forcing or hydrodynamic turbulence but it is solely generated by magnetic instabilities. The dynamo remains in this chaotic state for larger R_m for all the examined runs. Magnetic field energy continues to grow as R_m is further increased. This increase however appears to be logarithmic $E_b \sim \ln(R_m)$ or possibly a weak power law $E_n \sim R_m^{\delta}$ with $\delta < 0.15$. On the other hand, the kinetic energy is decreased approaching zero as R_m is increased. Note that at the largest examined value of R_m the magnetic energy is almost 2 orders of magnitude larger than the kinetic energy, and thus equipartition or sub-equipartition saturation mechanisms (see for example [31]) can be excluded in this limit.

Figure 2 shows the Ohmic (squares) and the viscous (diamonds) dissipation rate as a function of R_m. As the dynamo threshold is crossed the viscous dissipation rate is decreased and the Ohmic dissipation rate is increased. The total dissipation rate is smaller than the laminar no-dynamo dissipation rate (i.e., the system is less dissipative when the dynamo is turned on). The increase of the Ohmic dissipation rate continues until the critical value R'_{mc}, where the chaotic behavior starts. After this value both the viscous and the Ohmic dissipation rate are decreasing and become almost equal. This decrease continues up until the highest examined magnetic Reynolds number. Here, the results of the numerical simulations leave open the possibility that at infinite R_m a zero-injection, zero-dissipation state could be reached.

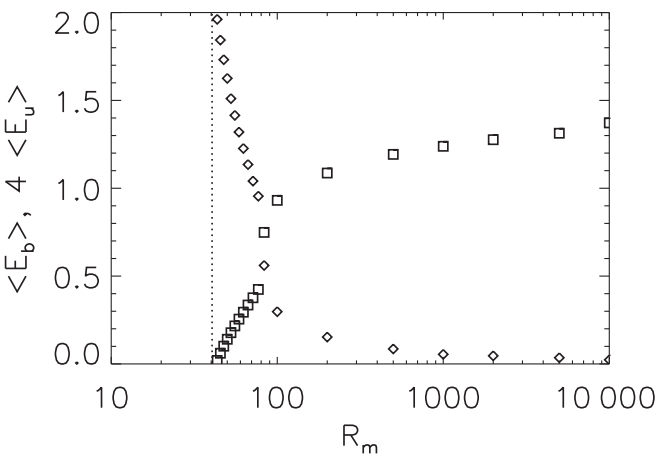

FIG. 1. Time averaged magnetic (squares) and kinetic (diamonds) energy as a function of R_m for the Archontis flow. The kinetic energy has been multiplied by a factor of 4 for reasons of clarity.

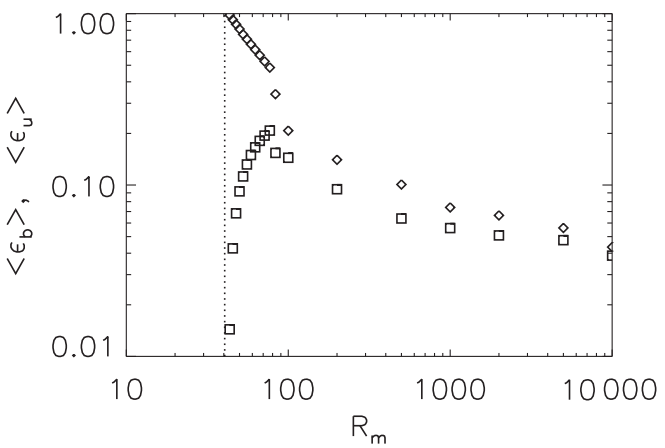

FIG. 2. Time averaged Ohmic (squares) and viscous (diamonds) dissipation rates as a function of R_m for the Archontis flow.

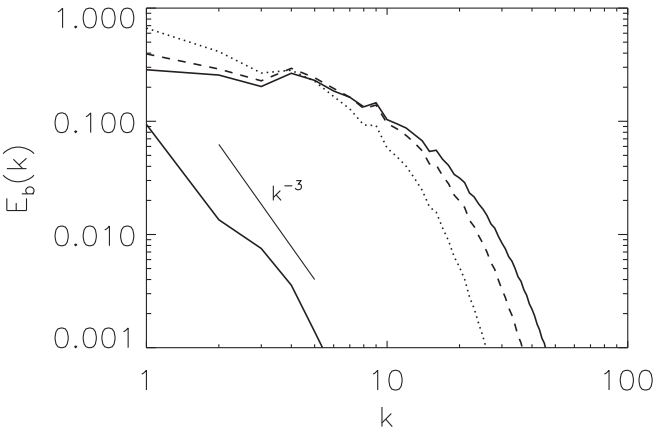

FIG. 3. Magnetic energy spectrum for three values of R_m: $R_m = 2000$ (dotted), $R_m = 5000$ (dashed), $R_m = 10000$ (solid) for the Archontis flow. The lower solid line shows the kinetic energy spectrum for $R_m = 10000$.

Finally, in Fig. 3 the energy spectra for the three largest examined values of R_m are shown. As expected the cutoff wave number due to magnetic diffusivity is increased as R_m is increased. What is also observed is that the bulk of the magnetic energy also moves from the large to the small scales as the magnetic Reynolds number is increased, with the slope of the spectrum changing from a negative value to almost flat. It should also be noted that the large scale magnetic energy is decreasing as R_m is increased while the total magnetic energy is increased.

Figure 4 shows magnetic energy density isosurfaces for the Archontis flow with $R_m = 10^4$. Most of the energy is concentrated in elongated almost two-dimensional structures. These structures have been reported before in kinematic dynamo simulations [24] and are referred to as "magnetic ribbons." Although these structures occupy a small fraction of the total volume they are responsible for almost bringing to a halt the flow in the entire domain.

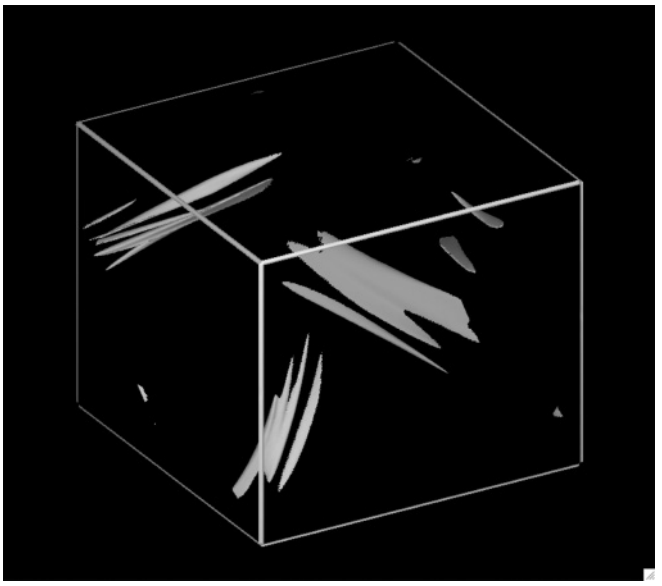

FIG. 4. Magnetic energy density isosurfaces for the Archontis flow; $R_m = 10^4$. The surfaces correspond to 50% of the maximum magnetic energy density or 10 times the average magnetic energy.

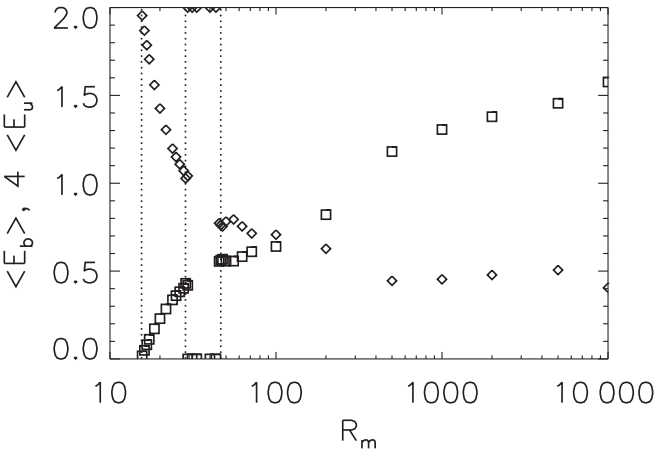

FIG. 5. Time averaged magnetic (squares) and kinetic (diamonds) energy as a function of R_m for the ABC, $k_f = 1$ flow. The kinetic energy has been multiplied by a factor of 4 for reasons of clarity.

B. ABC flow, $k_f = 1$

Next we examine the helical ABC flow forced at wave number $k_f = 1$. This is perhaps the most examined flow in periodic boxes for dynamo action. The onset of instability and the kinematic regime of the dynamo have been examined in Refs. [18–20]. It has been shown that the first onset of the dynamo is at $R_{mc1} \simeq 15.5$. This mode however stops being a dynamo when R_m becomes larger than $R_{mc2} \simeq 31$. A second unstable mode appears at $R_{mc3} = 43$ and the dynamo instability is present for all larger values of R_m.

Figure 5 shows the saturation levels of the magnetic (squares) and kinetic (diamonds) energy as a function of the magnetic Reynolds number. The dynamo instability begins at R_{mc1} as has been previously found and it exhibits a supercritical bifurcation. At the no-dynamo window between R_{mc2} and R_{mc3} the instability is subcritical at both ends of the window. This is revealed by the finite amplitude of saturation of the magnetic energy right at the onset of the instability. The extent of the subcriticality appears however to be very small: Nonlinear solutions with finite magnetic energy were found inside the no-dynamo window but very close to the boundaries of the window.

For larger values of R_m the magnetic energy continues to grow and this flow also exhibits chaotic behavior. As in the Archontis flow the magnetic energy shows a logarithmic (or a weak power law) increase with R_m. Unlike the Archontis flow however the kinetic energy saturates to a finite value $E_u \simeq 0.125$.

The Ohmic (squares) and viscous (diamonds) energy dissipation for the ABC dynamo is shown in Fig. 6 as a function of R_m. After the initial increase of the Ohmic dissipation at larger values of R_m, the two dissipations become almost independent of R_m with the viscous dissipation being twice as large as the Ohmic dissipation. As in the previously examined flow, in the presence of dynamo the system is less dissipative.

The magnetic energy spectra shown in Fig. 7 appear to have a positive slope at small wave numbers. This is in contrast with

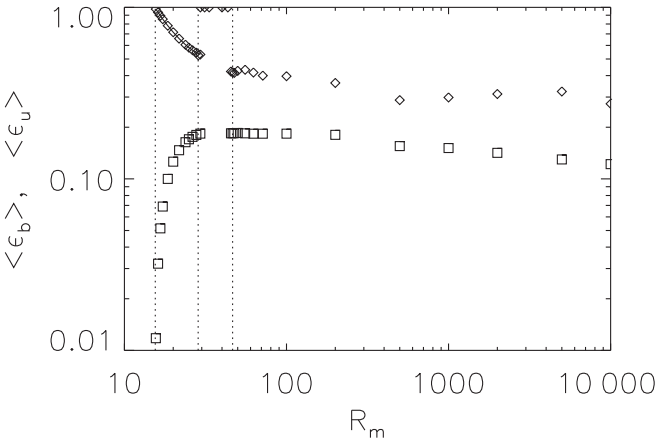

FIG. 6. Time averaged Ohmic (squares) and viscous (diamonds) dissipation rates as a function of R_m for the ABC, $k_f = 1$ flow.

the MHD simulations with order 1 Prandtl number for which at the saturated state most of the magnetic energy is concentrated close to the forcing scale [32,33]. The positive slope extends to larger wave numbers as the magnetic Reynolds number is increased.

The magnetic energy is concentrated in elongated structures as shown in Fig. 8. A gray-scale image of magnetic energy through the midplane of the box shown in Fig. 9 indicates more clearly that these structures are also flat and part of sheetlike structures that intensify in regions of strong shear; much like the the "ribbons" observed in the Archontis flow.

C. ABC flow, $k_f = 2$

Finally we examined the case for which the ABC flow is forced at wave number $k_f = 2$. The difference with the $k_f = 1$ case is that more magnetic modes are present in the system that move the onset of the instability to smaller values and allow magnetic helicity to concentrate in the large scales. Thus unlike the two previously examined cases that resulted in a weak amplitude of magnetic helicity, in this case magnetic helicity plays an important role.

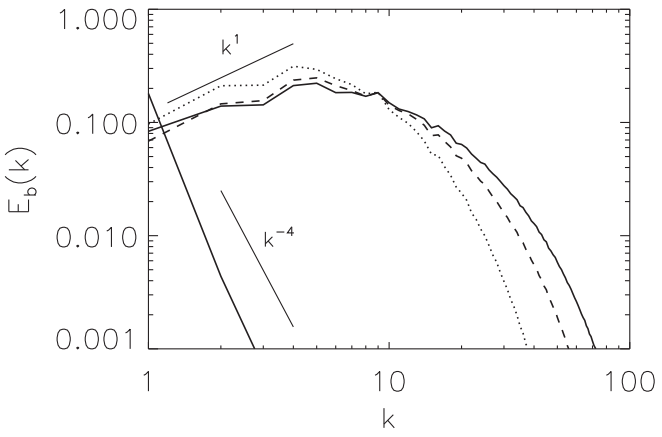

FIG. 7. Magnetic energy spectrum for three values of R_m: $R_m = 2000$ (dotted), $R_m = 5000$ (dashed), and $R_m = 10000$ (solid) for the ABC, $k_f = 1$ flow. The lower solid line shows the kinetic energy spectrum for $R_m = 10000$.

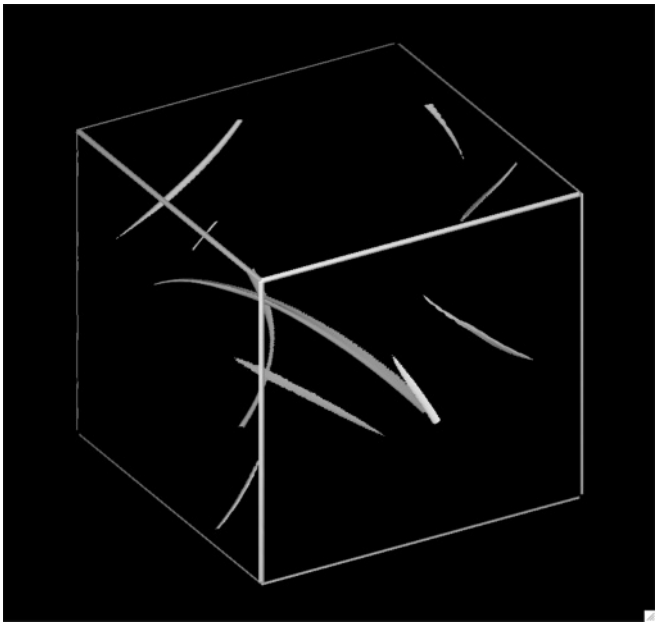

FIG. 8. Magnetic energy density isosurfaces for the ABC flow; $k_f = 1$, $R_m = 10^4$. The surfaces correspond to 50% of the maximum magnetic energy density or 10 times the average magnetic energy.

Figure 10 shows the magnetic (squares) and kinetic (diamonds) energy at saturation for this flow. The onset of the instability appears at $R_m \simeq 6$ and there is no no-dynamo window, unlike the $k_f = 1$ case. For large values of R_m the magnetic energy can be seen to increase at least as fast as the logarithm of the magnetic Reynolds number. This increase is more pronounced than the previously examined flows. The kinetic energy saturates at a finite value roughly equal to one-fifth of the value in the absence of dynamo.

FIG. 9. Gray-scale image of magnetic energy through the midplane $z = \pi$ of Fig. 8 (ABC flow, $k_f = 1$, $R_m = 10^4$). Bright regions indicate large magnetic energy.

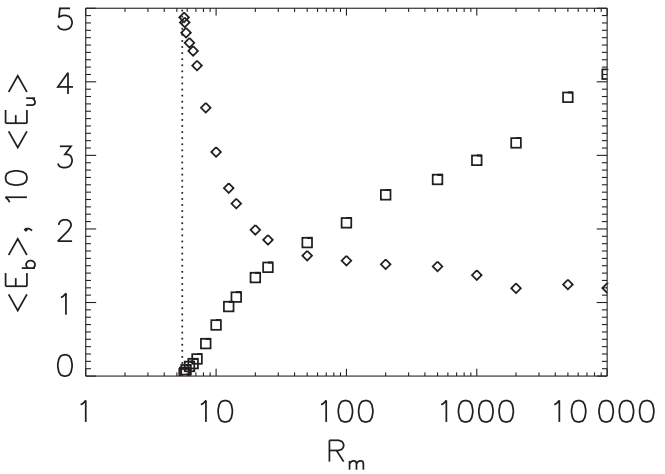

FIG. 10. Time averaged magnetic (squares) and kinetic (diamonds) energy as a function of R_m for the ABC, $k_f = 2$ flow. The kinetic energy has been multiplied by a factor of 10 for reasons of clarity.

The two dissipation rates Ohmic (squares) and viscous (diamonds) shown in Fig. 11 appear to be proportional for sufficiently large R_m with the Ohmic dissipation rate being roughly 4 times smaller than the viscous dissipation.

The most pronounced difference from the previous cases can be seen in the magnetic energy spectra (Fig. 12). Unlike the previously examined cases the bulk of the magnetic energy is concentrated at the large scales as a result of the inverse cascade of the magnetic helicity [34–39]. In the small scales the energy spectrum appears to follow a power-law behavior $E_b(k) \sim k^{\alpha}$ with an exponent close to $\alpha = -1$.

The magnetic and kinetic helicity as a function of R_m is shown in Fig. 13. The last three points in this figure were obtained from the numerical simulations after roughly one diffusion time where the magnetic helicity was still slightly increasing with time. To obtain a well converged averaged value many diffusion times would be required, which is not feasible with the present computational power.Thus for these points the saturated value of the magnetic helicity is expected to be slightly higher than what is shown in Fig. 13. From

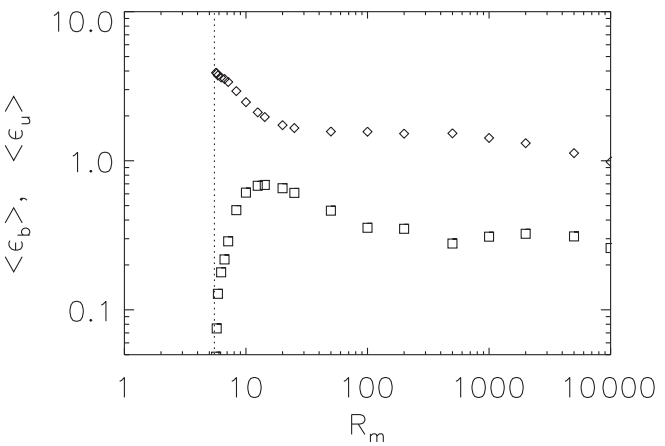

FIG. 11. Time averaged Ohmic (squares) and viscous (diamonds) dissipation rates as a function of R_m for the ABC, $k_f = 2$ flow.

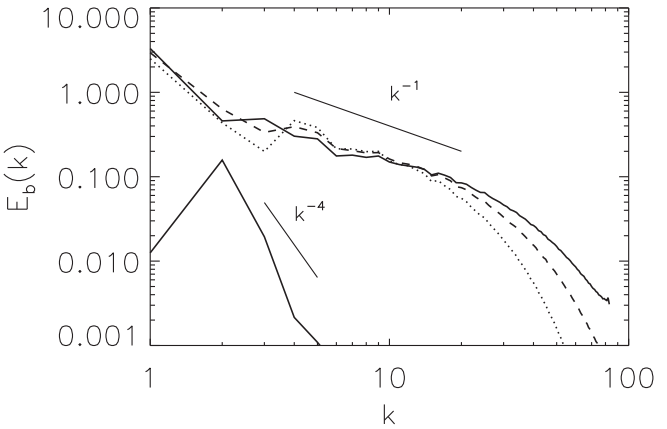

FIG. 12. Magnetic energy spectrum for three values of R_m: $R_m = 2000$ (dotted), $R_m = 5000$ (dashed), and $R_m = 10000$ (solid) for the ABC, $k_f = 2$ flow. The lower solid line shows the kinetic energy spectrum for $R_m = 10000$.

the figure however one can see that the saturated value of the magnetic helicity is slowly increasing with R_m while hydrodynamic helicity is approaching an asymptotic value. As discussed in the introduction this positive value of magnetic helicity implies that negative helicity has cascaded to the small scales where it was dissipated while positive helicity was concentrated at the large scales. At the nonlinear stage the flow is altered so that although still helical (see Fig. 13) it is less efficient at generating large scale helicity. The spectrum of the magnetic helicity is shown in Fig. 14. Unlike the kinematic stage in which negative helicity is concentrated in the small scales and positive in the large, at saturation helicity has the same sign in both large and small scales. This implies that at the nonlinear stage some of the large scale helicity has been cascaded to the small scales. The transfer of the large scale helicity to the small scales has been observed in MHD simulations where a scale to scale transfer of the magnetic helicity was investigated [39]. It is also noted that the helicity spectrum is very steep. If the magnetic field was fully helical at small scales then it would be expected that the helicity spectrum would scale like $H_m \sim E_b/k \sim k^{-2}$, but in Fig. 14

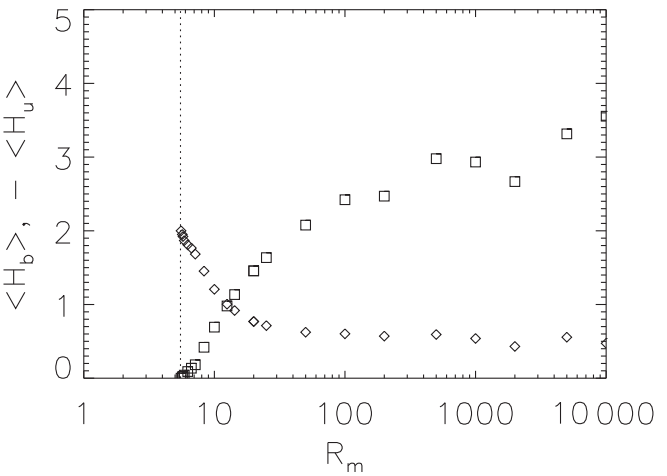

FIG. 13. Time averaged magnetic (squares) and kinetic (diamonds) helicity as a function of R_m for the ABC, $k_f = 2$ flow.

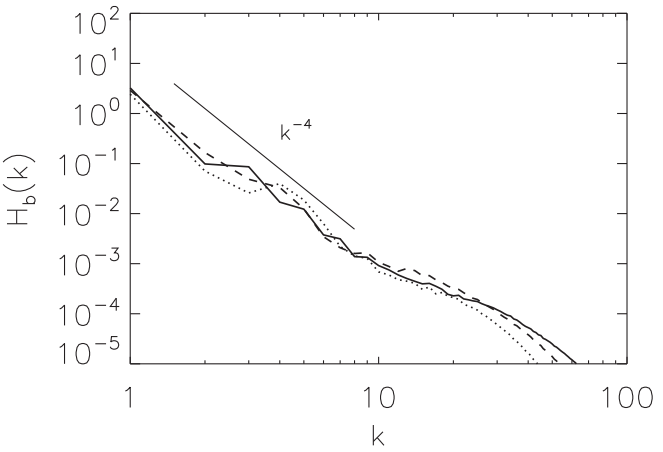

FIG. 14. Magnetic helicity spectrum for three values of R_m: $R_m = 2000$ (dotted), $R_m = 5000$ (dashed), and $R_m = 10000$ (solid) for the ABC, $k_f = 2$ flow.

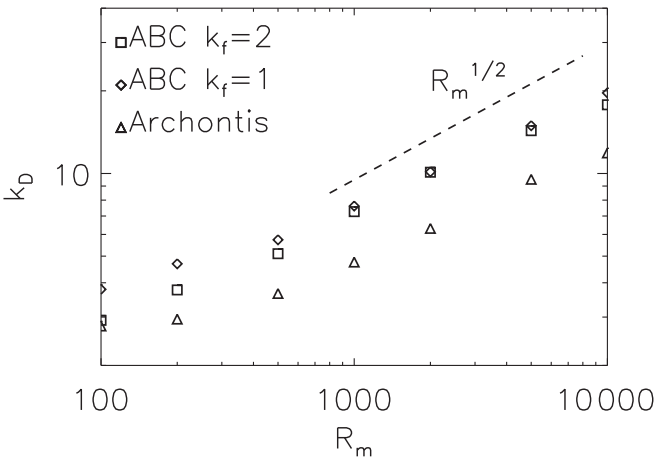

FIG. 16. Magnetic energy dissipation wave number k_D as a function of R_m.

the slope is much steeper ($H_m \sim k^{-4}$) implying that both signs of helicity are present in the small scales with the positive sign only slightly dominating.

The magnetic structures that appear for this flow can be seen in Fig. 15 where magnetic energy density isosurfaces are shown. Again here energy is concentrated in long and flat structures (ribbons). Although small scale structures are also present here they appear to be more "organized" to form large scale patterns. Note the twisting of the "ribbons" that indicates the presence of helicity.

V. SCALINGS AT SATURATION

The three examined flows have some common features that are worth further exploring. One of the fundamental relations from the kinematic theory that has been shown to hold for a variety of flows is that during the kinematic stage the stretching term that scales like $\sim UB/\ell_U$ (where U, B, ℓ_U are typical velocity, magnetic field, and velocity length scale respectively) is balanced by the magnetic diffusion term that scales like $\sim \eta B/\ell_D^2$ (where ℓ_D is the diffusion length scale). This relation leads to the prediction that $\ell_D \sim \ell_U/\sqrt{R_m}$. This relation continues to hold at the saturated stage. Figure 16 shows the dissipation wave number $k_D \sim 1/\ell_D$ (defined as $k_D^2 = \langle(\nabla \mathbf{b})^2\rangle/\langle \mathbf{b}^2\rangle$) as a function of R_m. For sufficiently large R_m for all flows the dissipation wave number follows a scaling close to $k_D \sim R_m^{1/2}$. (A best fit gives a value of the exponent closer to $k_D \sim R_m^{0.4}$). The velocity length scale on the other hand appears to depend weakly on the magnetic Reynolds number. In Fig. 17 we plot the ratio of the velocity wave number $k_U^2 = \langle(\nabla \mathbf{u})^2\rangle/\langle \mathbf{u}^2\rangle \sim \ell_U^{-2}$ to the forcing wave number k_f. k_U for the two ABC flows appears to be almost independent of R_m and close to k_f. For the Archontis flow the velocity wave number is weakly increasing with R_m. Thus at the nonlinear stage both length scales ℓ_D and ℓ_U follow a similar scaling with R_m as they do in the the linear stage. Furthermore this scaling also explains why the Ohmic dissipation that scales

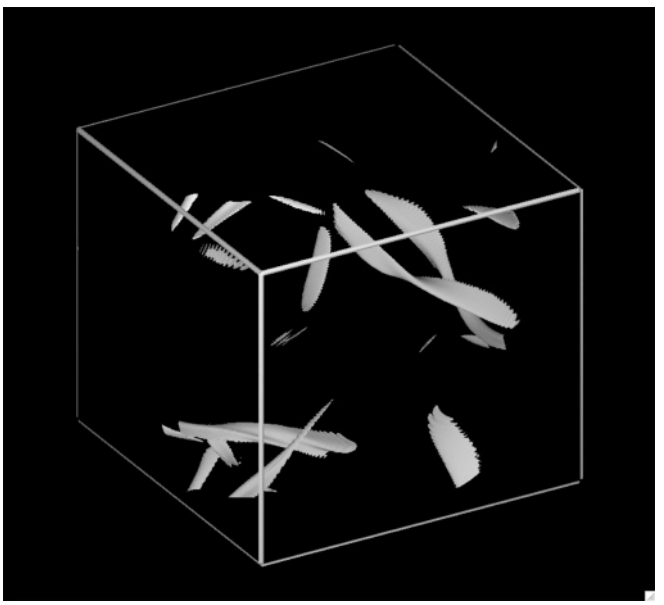

FIG. 15. Magnetic energy density isosurfaces for the ABC, $k_f = 2$ flow; $R_m = 10^4$. The surfaces correspond to 50% of the maximum magnetic energy density or 10 times the average magnetic energy.

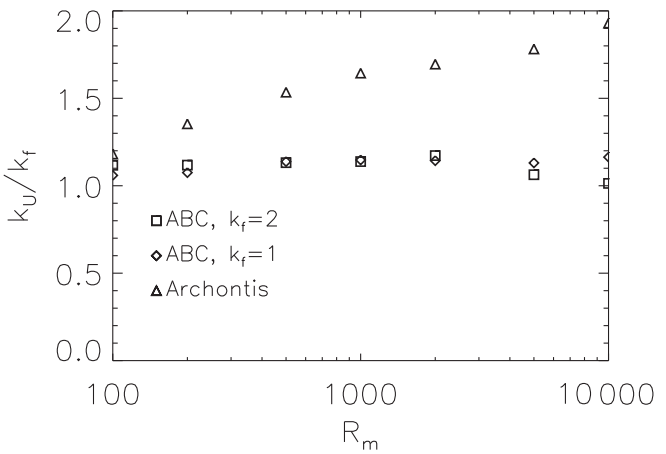

FIG. 17. The kinetic energy dissipation wave number k_U as a function of R_m.

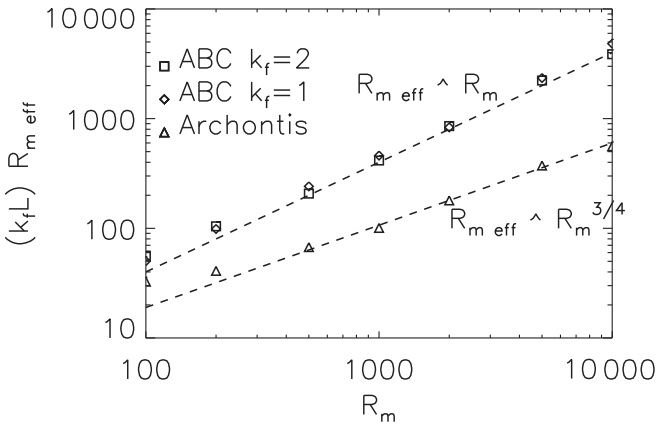

FIG. 18. The effective magnetic Reynolds number R_{meff} (based on the velocity amplitude and length scale at the nonlinear stage) as a function of R_m for the three different flows.

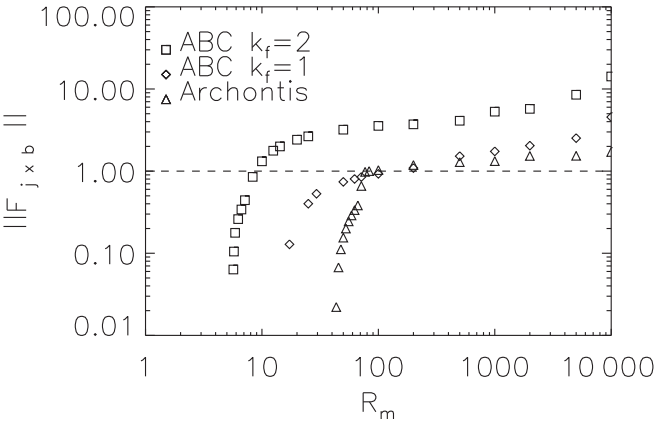

FIG. 19. The amplitude of the Lorentz force for the three different flows as a function of R_m.

like $\epsilon_b \sim B^2/R_m \ell_D^2$ is of the same order with the viscous dissipation that scales like $\epsilon_u \sim U^2/\ell_U^2$.

Besides the two length scales it is also interesting to investigate the effect of saturation on the magnetic Reynolds number. An effective magnetic Reynolds number at saturation can be defined as $R_{meff} = U_{nl}/k_U \eta$, where $U_{nl} = (2E_u)^{1/2}$ is the velocity amplitude at the nonlinear stage and k_U the velocity wave number as defined in the previous paragraph. If the dynamo saturates by decreasing the effective Reynolds number at the nonlinear stage then it would be expected that as R_m is increased, R_{meff} would approach the onset value R_{mc}.

In Fig. 18 we plot the effective Reynolds number as a function of R_m. For the ABC flows the relation between the two Reynolds numbers is very close to linear. For the Archontis flow the R_{meff} is increasing with R_m but weaker than linear and closer to the scaling $R_{meff} \sim R_m^{3/4}$. This weaker slope is due to the decrease of the the kinetic energy at the nonlinear stage. It appears thus that for the Archontis flow the magnetic field configuration cancels the external body force almost perfectly up to small fluctuations while for the two ABC flows this is not achievable and strong fluctuations exist. Figure 18 then implies that all relations described in this work for R_m hold also for R_{meff} for the ABC flows, and for the Archontis flow provided the rescaling $R_{meff} \sim R_m^{3/4}$ is taken into account. Finally since R_{meff} is increasing with R_m saturation is not solely due to the decrease of the amplitude of the velocity.

Although the magnetic field does not modify significantly the amplitude of the flow to saturate the dynamo it does modify its structure. A measure of the strength of this modification is given by the amplitude of the solenoidal projection of the Lorentz force $F_{j\times b} = \mathbf{b}\cdot\nabla\mathbf{b} - \nabla P$. Figure 19 shows the amplitude $\|F_{j\times b}\| = \langle F_{j\times b}^2\rangle^{1/2}$ as a function of R_m. What is observed is that for moderate values of $R_m (50 < R_m < 1000)$ the amplitude of the Lorentz force is close to the forcing amplitude ($\|\mathbf{F}\| = 1$). As R_m is further increased the amplitude of $F_{j\times b}$ seems to increase to larger values for the two ABC flows, while a weaker increase is observed for the Archontis flow. This suggests that at least for moderate R_m, $F_{j\times b}$ is in balance the body force F. At larger R_m the effect of the Lorentz force is probably less organized due to the presence of fluctuations, and larger amplitudes of $\|F_{j\times b}\|$ are needed to achieve a balance with F.

One then needs to explain how a balance between a force generated by a small scale magnetic field (ℓ_D) and a large scale force (ℓ_U) is achieved. In Fig. 20 we show the relative amplitude of $\|F_{j\times b}\|$ normalized by the amplitude of the current density $\|j\| = \langle(\nabla\times b)^2\rangle^{1/2}$ and magnetic field amplitude $\|b\| = \langle b^2\rangle^{1/2}$ as a function of the magnetic Reynolds number. If the two fields $\mathbf{b}$ and $\mathbf{j} = \nabla\times\mathbf{b}$ were randomly organized, the quantity $\|F_{j\times b}\|/(\|j\|\|b\|)$ should be of order 1. If however the two fields were aligned or were organized so that their cross product is a potential field the relative amplitude of $\|F_{j\times b}\|$ can be a lot smaller. In Fig. 20 the relative amplitude of the Lorentz force appears to decrease as a power law for all flows with exponent close to $\|F_{j\times b}\| \sim R_m^{-1/2}\|j\|\|b\|$. (A best fit gives a value of the exponent closer to -0.4.) This can be understood in the following way. Saturation is expected to be achieved when the Lorentz force is of the same order with the external forcing $F \sim F_{j\times b} = O(1)$. The amplitude of the Lorentz force is also expected to scale as $F_{j\times b} \sim f\|j\|\|b\|$ where f is a prefactor that depends on the alignment and structure of the two fields. Since the current density amplitude is controlled by the balance of stretching and diffusion as seen in Fig. 16, we expect

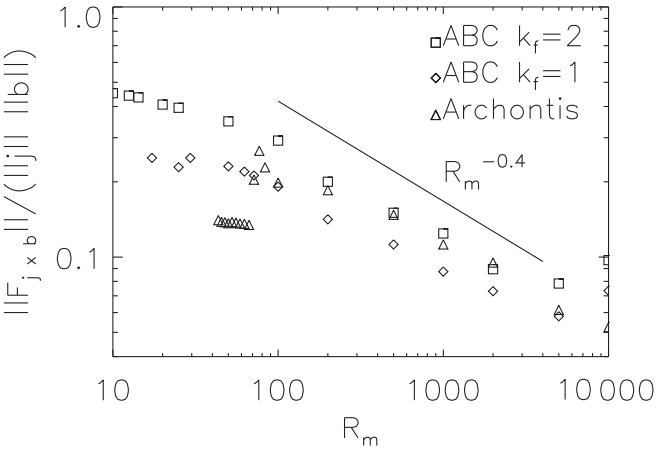

FIG. 20. The amplitude of the Lorentz force normalized by $\|j\|\|b\|$ for the three different flows as a function of R_m.

the scaling $\|j\| \sim \|b\| R_m^{1/2}/L$. Equating the two relations we obtain that for an order 1 magnetic field the prefactor f must scale like $R_m^{-1/2}$. This implies that the magnetic field must come close to a force-free configuration as R_m is increased.

There are many ways to construct a force-free magnetic field. Perhaps the simplest way is by making the two fields **b** and **j** aligned and thus have zero cross product. However, the alignment of **b** and **j** measured in the simulations is not sufficient to explain the decrease of the relative amplitude of $\|F_{j\times b}\|$. The cross product of the two fields is not small but it is close to a potential flow and thus has a small solenoidal projection. This is achieved by forming the flat structures observed in Figs. 4, 9, and 15. In these structures both **b** and **j** lie on a flat surface (say $\mathbf{b} \sim \hat{\mathbf{x}} b$ and $\mathbf{j} \sim \hat{\mathbf{y}} j$) while they vary fast in the perpendicular direction (say $\hat{\mathbf{z}}$). Thus their cross product $\mathbf{j} \times \mathbf{b}$ is along the fast varying direction perpendicular to surface ($\hat{\mathbf{z}}$) and can be balanced by a pressure field $P(z)$. In this way although $F_{j\times b}$ is formed by small scale fields it varies on a much longer length scale that is proportional to the curvature of the structures which is of the order of the forcing scale and not their thickness which is much smaller.

The observed deviations from this balance as R_m is increased only reflect that $F_{j\times b} \sim F$ is not satisfied due to the presence of fluctuations that require $\|F_{j\times b}\| > \|F\|$ and thus stronger magnetic field to achieve saturation. The behavior of these fluctuations due to magnetic instabilities thus seems to play an important role in the saturation at high R_m and needs to be studied further.

VI. SUMMARY AND DISCUSSION

The nonlinear behavior of the dynamo instability was investigated in the infinite Prandtl number limit for three different stationary flows. In this limit large values of R_m can be examined at moderate resolutions and this allowed us to investigate how the nonlinear behavior of the dynamo scales with R_m. What was shown for all flows is that the magnetic energy is increasing with R_m at least logarithmically. This increase was most pronounced for the ABC flow forced at $k_f = 2$ for which an inverse cascade of magnetic helicity was present. The Ohmic and viscous dissipation rates on the other hand varied in behavior. For the two ABC flows they were approaching an asymptotic value as R_m was increased while for the Archontis flow were slowly decreasing R_m. For all flows however the Ohmic and viscous dissipation rates although operating at different scales were of the same order as a result of the balance between stretching and diffusion.

The saturation of the dynamo comes from a balance between the Lorentz force and the external body force as their similar amplitudes suggest. At saturation the magnetic field forms elongated flat structures whose thickness scales like $R_m^{-1/2}$. The typical length scale along the other directions was of the order of the forcing length scale. These structures were almost force free with the solenoidal projection of the Lorentz force scaling like $F_{j\times b} \sim \|j\|\|b\|/\sqrt{R_m}$. This decrease of $F_{j\times b}$ is the result of the organization of the magnetic field in these flat structures. The cross product of the magnetic field with the current in these flat structures results in a field that is both pointing and varying in the direction perpendicular to the surface, and thus is close to a potential field. In this way the magnetic field is successful in balancing the external force that differs both in amplitude (compared to B^2/l_D) and length scale.

Another common feature that all flows had was that the generated structures were unstable to small scale fluctuations that resulted in a chaotic behavior. Note that these fluctuations are due to magnetic instabilities and their origin is probably related to reconnection events. However, these chaotic fluctuations have not resulted in universal spectra. The observed slopes of the spectra varied from positive (ABC $k_f = 1$ flow) to almost flat spectrum (Archontis flow) to negative slope (ABC $k_f = 2$ flow). Thus if these instabilities lead to universal behavior it must happen for even larger magnetic Reynolds numbers.

Finally, a comment needs to be made regarding the applicability of these results to realistic flows. Although the dynamo has been investigated in a somewhat idealistic limit some insight can be gained. In a realistic flow there exists both large scale structured flows forced by a thermal or other instability and turbulent small scale fluctuations as a result of a turbulent cascade. Although the turbulent fluctuations result in the fastest growing modes in a large Prandtl number dynamo flow at saturation the magnetic field configuration must be such that the Lorentz force prevents further magnetic field amplification due to both the turbulent fluctuations and the large forcing scales. The results in this work help in understanding the latter behavior. In particular this work gives a clear example of how small scale fields can organize themselves to come in balance with a large scale forcing.

ACKNOWLEDGMENTS

The author would like to thank F. Petrelis and S. Fauve for useful discussions and two anonymous referees for their comments. Computations were carried out on the CEMAG computing center at LRA/ENS and on the CINES computing center, and their support is greatly acknowledged.

[1] Ya. B. Zeldovich, A. A. Ruzmaikin, and D. D. Sokoloff, *Magnetic Fields in Astrophysics* (Gordon & Breach, London, 1990).

[2] F. Cattaneo, D. W. Hughes, and E. J. Kim, Phys. Rev. Lett. **76**, 2057 (1996).

[3] J. Maksymczuk and A. D. Gilbert, Geophys. Astrophys. Fluid Dyn. **90**, 127 (1998).

[4] F. Cattaneo and S. M. Tobias, J. Fluid Mech. **621**, 205 (2009).

[5] A. Tilgner and A. Brandenburg, Mon. Not. R. Astron. Soc. **391**, 1477 (2008).

[6] M. Schrinner, D. Schmitt, R. Cameron, and P. Hoyng, Geophys. J. Int. **182**, 675 (2010).

[7] A. Courvoisier, D. W. Hughes, and M. R. E. Proctor, Proc. R. Soc. London A **466**, 583 (2010).

[8] A. A. Schekochihin, S. C. Cowley, S. F. Taylor, G. W. Hammett, J. L. Maron, and J. C. McWilliams, Phys. Rev. Lett. **92**, 084504 (2004).
[9] A. A. Schekochihin, S. C. Cowley, and J. L. Maron, Phys. Rev. Lett. **92**, 064501 (2004).
[10] A. A. Schekochihin, J. L. Maron, S. C. Cowley, and J. C. McWilliams, Astrophys. J. **576**, 806 (2002).
[11] A. A. Schekochihin, S. C. Cowley, and J. L. Maron, Phys. Rev. E **65**, 016305 (2001).
[12] H. K. Moffatt, J. Fluid Mech. **35**, 117 (1969).
[13] D. O. Gomez, P. D. Mininni, and P. Dmitruk, Adv. Space Res. **35**, 899 (2005).
[14] D. O. Gomez, P. D. Mininni, and P. Dmitruk, Phys. Scr. T **116**, 123 (2005).
[15] V. I. Arnold, C. R. Acad. Sci. Paris **261**, 17 (1965).
[16] T. Dombre, U. Frisch, J. M. Greene, M. Henon, A. Mehr, and A. M. Soward, J. Fluid Mech. **167**, 353 (1986).
[17] O. M. Podvigina and A. Pouquet, Physica D **75**, 471 (1994).
[18] V. I. Arnold and E. I. Korkina, Vestn. Mosk. Univ., Ser. 1: Mat, Mekh. **3**, 43 (1983).
[19] D. J. Galloway and U. Frisch, Geophys. Astrophys. Fluid Dyn. **36**, 53 (1986).
[20] Y. T. Lau and J. M. Finn, Phys. Fluids B **5**, 365 (1993).
[21] S. Childress and A. D. Gilbert, *Stretch, Twist, Fold: The Fast Dynamo* (Springer, New York, 1995).
[22] D. J. Galloway and M. R. E. Proctor, Nature (London) **356**, 691 (1992).
[23] V. Archontis, Ph.D. thesis, Copenhagen University, 2000.
[24] V. Archontis, S. B. F. Dorch, and A. Nordlund, Astron. Astrophys. **397**, 393 (2003).
[25] S. B. F. Dorch and V. Archontis, Sol. Phys. **224**, 171 (2004).
[26] V. Archontis, S. B. F. Dorch, and A. Nordlund, Astron. Astrophys. **472**, 715 (2007).
[27] R. Cameron and D. Galloway, Mon. Not. R. Astron. Soc. **365**, 735 (2006).
[28] A. D. Gilbert, Y. Ponty, and V. Zheligovsky, DOI: 10.1080/03091929.2010.513332.
[29] S. Fauve and F. Petrelis, C. R. Phys. **8**, 87 (2007).
[30] S. Fauve and F. Petrelis, Eur. Phys. J. B **22**, 273 (2001).
[31] S. I. Vainstein and F. Cattaneo, Astrophys. J. **393**, 165 (1992).
[32] P. D. Mininni, Y. Ponty, D. C. Montgomery, J.-F. Pinton, H. Politano, and A. Pouquet, Astrophys. J. **626**, 853 (2005).
[33] D. O. Gomez and P. D. Mininni, Nonlin. Processes Geophys. **11**, 619 (2004).
[34] A. Pouquet, U. Frisch, and J. Leorat, J. Fluid Mech. **77**, 321 (1976).
[35] A. D. Gilbert and P. L. Sulem, Geophys. Astrophys. Fluid Dyn. **51**, 243 (1990).
[36] A. Brandenburg, Astrophys. J. **550**, 824 (2001).
[37] A. Brandenburg, W. Dobler, and K. Subramanian, Astron. Nachr. **323**, 99 (2002).
[38] A. D. Gilbert, Geophys. Astrophys. Fluid Dyn. **96**, 135 (2002).
[39] A. Alexakis, P. D. Mininni, and A. Pouquet, Astrophys. J. **640**, 335 (2006).